Volume 5
Number 2
February 2026
Pages 133–242

Energy Advances

rsc.li/energy-advances

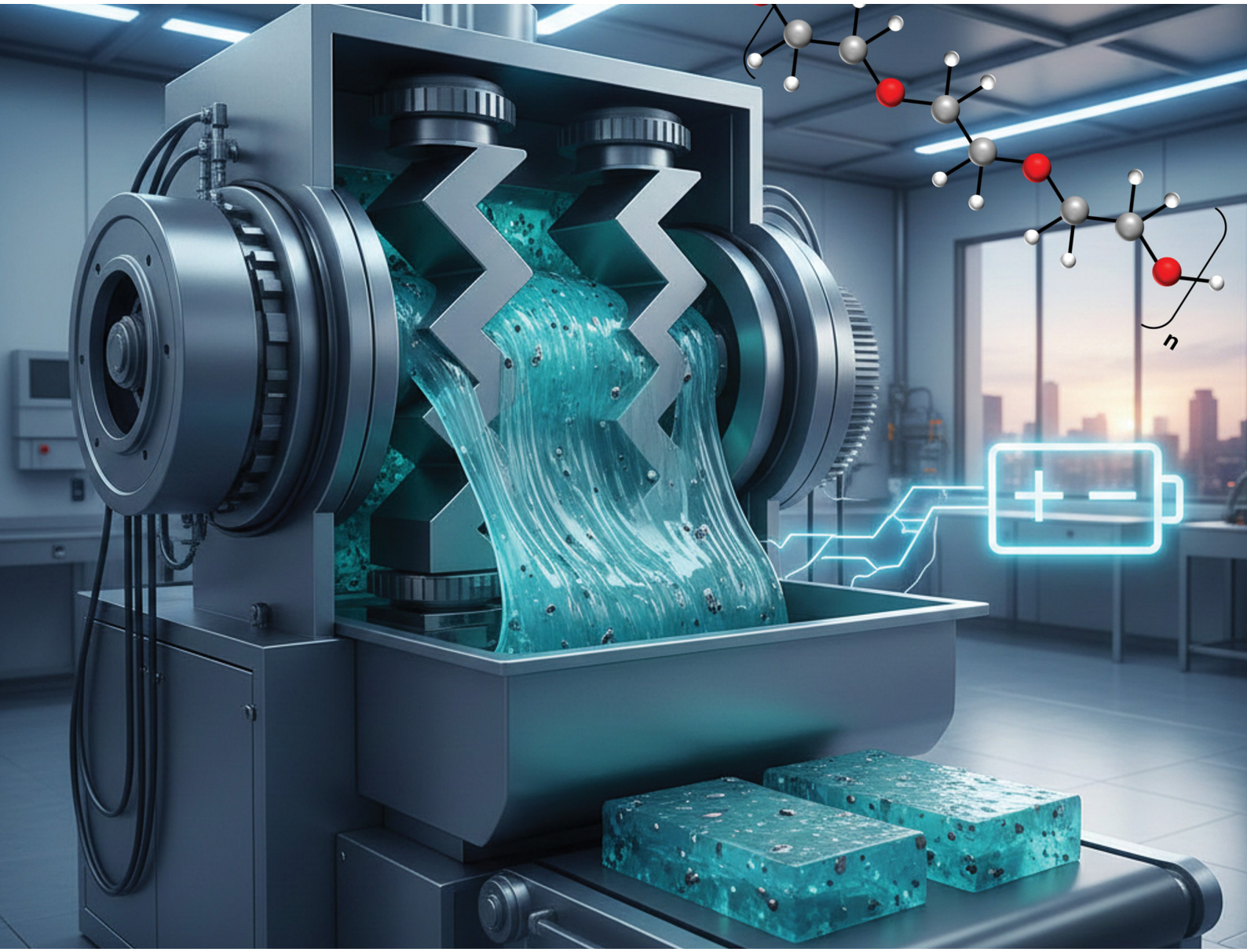

ISSN 2753-1457

ROYAL SOCIETY OF CHEMISTRY

PAPER

G. Garnweitner *et al.*

Simple and scalable solvent-free PEO based electrolyte fabrication by kneading for all solid state lithium sulfur batteries

Energy Advances

ROYAL SOCIETY OF CHEMISTRY

PAPER

View Article Online
View Journal | View Issue

Cite this: *Energy Adv.*, 2026, 5, 151

Simple and scalable solvent-free PEO based electrolyte fabrication by kneading for all solid state lithium sulfur batteries

N. L. Grotkopp,[ab] M. Hokmabadi,[ab] M. Nebelsiek,[bc] M. Kurrat,[bc] P. Michalowski,[ab] A. Jean-Fulcrand[abd] and G. Garnweitner *[ab]

Received 10th October 2025,
Accepted 26th November 2025

DOI: 10.1039/d5ya00294j

rsc.li/energy-advances

PEO is the most investigated polymer for battery solid electrolytes, and continues to be considered state of the art to this day. It is often prepared by tape casting in a solvent-based process. However, solvent-free production of battery electrolytes has become a prominent topic in the recent years in science and industry. This is due to the elimination of one process step – the evaporation of a solvent – sparing production time, material, energy, solvent disposal and thus substantially reducing the production costs. Herein we propose the quick and simple solvent-free preparation of a PEO-LiTFSI electrolyte by kneading on a larger scale with reduced production times compared to conventional solvent based techniques. 50 g of electrolyte are produced at 60 °C within ~15 min of kneading and another ~5 min for calendering at 120 °C, whilst for the solvent-based solid electrolyte processing, ~1.5 h followed by drying over night was required to prepare one solid electrolyte film. The processing and properties of the electrolyte are thoroughly discussed, comparing different conducting salts, polymer molecular weights and polymer–salt concentrations that are evaluated by EIS at different temperatures. An SEM and 4K light microscope-supported post mortem analysis was performed to provide insights on the surface processes of the electrodes that occur during galvanostatic cycling. Moreover, we report the first application of this solvent-free based PEO solid electrolyte in Li–S cells with different electrolyte thicknesses at 50 °C.

1. Introduction

With its high specific energy (theoretically amounting to 2600 Wh kg^{-1}), the lithium sulfur (Li–S) battery technology gains more and more interest for application in the modern transportation industry.[1–3] Especially for short-range aviation and drones a lightweight energy supply system possessing high gravimetric energy density is necessary.[4–6] In the aviation industry, the safety of a battery system becomes of high importance. Thus, batteries based on liquid electrolytes are considered hazardous mainly because of their susceptibility to ignition upon short circuiting, as well as due to leakage concerns, possible dry-out, evaporation and thermal runaway, which shifted the interest towards solid state batteries (SSB).[7–11] Solid polymer electrolytes are highly promising due to their broad availability and mechanical flexibility leading to good processability and low contact resistance. With respect to the scalability of such desired solid electrolytes, one impactful aspect is minimizing the use of solvents, as their removal involves expensive additional processing steps, which create issues related to environmentally responsible waste disposal and maintaining a safe work environment.[12,13] Completely solvent-free electrolyte processing circumvents these problematic aspects and can for example be realized by using a kneader.[14] When speaking about scalability also the material costs cannot be neglected. Most of battery related research is performed under laboratory conditions that are difficult to be scaled up, especially when rare and sensitive materials are involved.[15,16] Therefore, there is a preference for using cost-effective blends of electrolyte matrix and conducting salt that offer both functionality and economic viability. One of the most investigated SSB polymer materials is PEO. When combined with conducting salts, it provides sufficient ionic conductivity above 50 °C, making it suitable for galvanostatic cycling.[17] PEO remains an extensively studied polymer electrolyte material in current battery research, because of its straightforward

[a] *Institute for Particle Technology, Technische Universität Braunschweig, 38104 Braunschweig, Germany. E-mail: g.garnweitner@tu-braunschweig.de*
[b] *Battery LabFactory Braunschweig (BLB), Technische Universität Braunschweig, 38106 Braunschweig, Germany*
[c] *Elenia Institute of High Voltage Technology and Power Systems, Technische Universität Braunschweig, 38106 Braunschweig, Germany*
[d] *General Education Department, École de Technologie Supérieure, 1100, rue Notre-Dame Ouest, Montréal, H3C 1K3, Québec, Canada*

processing, relatively high ionic conductivity, wide availability, cost effectiveness, high lithium (Li) salt solubility, and its flexibility enhancing interfacial contact.[18–23] Whilst a number of works have investigated the use of PEO of different molecular weight as well as different Li salts on the ionic conductivity and electrochemical performance, systematic studies are largely lacking, and the correlation of electrolyte composition to its performance is unknown. Therefore, empirical optimizations regarding material properties to improve ionic conductivity are required, along with post mortem analysis to enable an in-depth understanding of component behavior during galvanostatic cycling and particularly in terms of compatibility with the highly reactive lithium metal anode.

In this research, we report a systematic analysis of the use of PEO-based solid electrolytes in Li–S SSB, utilizing different molecular weights of PEO as well as various conducting salts and salt-polymer concentration ratios (EO : Li) at different temperatures. Subsequently, the solvent-free production of the solid electrolyte identified to show best properties was established by using a kneader allowing a larger scale and reduced production times compared to conventional solvent-based methods. The fabrication of solid electrolytes by kneading has been previously investigated at our institution, whilst not under an optimization of the electrolyte composition, neither a comparison of different PEO polymer molecular weights (chain lengths) nor a variation or optimization of the electrolyte composition were performed.[14,24,25] Here, for the first time the PEO-based solid electrolyte made under solvent-free conditions was applied to lithium-metal-sulfur batteries. Furthermore, the challenges associated with post-mortem analysis of Li–S-cells using PEO based solid electrolyte, primarily due to the electrolyte's stickiness, is demonstrated. This difficulty explains the still limited literature available on this topic. We show a comprehensive post-mortem analysis, supported by SEM and 4K light microscopy of Li–S EL-cells, which clarifies the degradation process and reveals that cell malfunctioning could be attributed to lithium dendrite formation.

2. Experimental

For experimental work conducted under dry conditions, a dry room with a dew point between −40 and −60 °C (Battery LabFactory Braunschweig, Germany) was used.

2.1. Electrolyte preparation

For comparison, solvent-based electrolyte preparation was carried out in the dry room by dissolving the conducting salts LiTFSI (lithium bis(trifluoromethanesulfonyl)imide, 99.9%, water content max. 20 ppm, Solvionic SA), LiFSI (lithium bis(fluorosulfonyl)imide, 99.9%, water content max. 20 ppm, Solvionic SA) or LiBArF (lithium tetrakis(pentafluorophenyl)borate, 98%, BLD Pharmatech GmbH) in acetonitrile (≥99.8%, water content max. 10 ppm, VWR International) using a dissolver (Dispermat TU, VMA-Getzmann GmbH, Germany). PEO of five different average molecular weights (2000, 20 000, 200 000, 600 000 and 2000 000 Da) was used. Thereby, the PEO with 2000–200 000, 2000 000 Da was procured from Merck KGaA, whilst the PEO with 600 000 Da was POLYOX™ WSR 205 from The DOW Chemical Company. All polymers were previously dried for 24 h at 40 °C and then mixed into the acetonitrile solution resulting in a homogeneous solution, except for LiBArF. In the latter case, a homogenous solution of LiBArF was prepared by using ethanol (anhydrous, ≥99.8%, VWR International) as a solvent. The dispersion parameters of the dissolver are initially a stirring rate of 800 rpm for 10 min followed by mixing at 230 rpm for 1 h. Three different EO : Li ratios (10 : 1, 15 : 1 and 20 : 1) were investigated for each tested conducting salt. All solutions contained air bubbles which were eliminated by evacuation inside a desiccator. In some cases, the air bubbles on the surface had to be burst with a spatula for complete removal. Subsequently, casting was performed by applying the homogeneous solution onto an anti-adhesive siliconized polyester foil (36 μm, one side coated, PPI Adhesives Products GmbH) on a tape-casting device (Zehntner GmbH Testing Instruments, ZAA 2300, Switzerland) and spreading it with a casting blade (Zehntner GmbH Testing Instruments, ZUA 2000, Switzerland). After a first drying step at 30 °C, the remaining solvent was evaporated in a vacuum oven (Binder Modell VD 115, BINDER GmbH, Germany) at 40 °C over night. The resulting films can be delaminated from the substrate foil and are thus considered free-standing. For storage, all samples were sealed in aluminum bags.

Solvent-free electrolyte preparation was carried out in the same dry room by kneading (Rheomix 600 kneader, Thermo Scientific) PEO 600 000 Da with LiTFSI in a 12 : 1 EO : Li ratio at 60 °C. First the material was fed at 5 rpm and premixed for 5 minutes. Afterwards the speed was increased to 60 rpm for 10 minutes. The resulting product was then pre-pressed using a hot press at 60 °C (VOGT Labormaschinen GmbH, LaboPress P200 S, Germany). The pre-pressed electrolyte sheet was further densified by a calender (MWG 300 L, Saueressig Group, Germany) at 120 °C and 0.5 m min^{-1} using different roll-to-roll gaps resulting in homogeneous films with thicknesses of 150, 300 and 600 μm (±5 μm).

2.2. Materials characterization

Scanning electron microscopy (SEM) (Thermo Fisher Scientific, Helios G4 CX Dual-Beam, USA) was performed to investigate the morphology of the Li anode and S cathode after post-mortem analysis. Energy dispersive X-ray spectroscopy (EDX) (Octane Elite-70, EDAX, Mahwah, NJ, United States) was conducted for elemental analysis. For sample transfer, the Li anode and S cathode were prepared in the dry room onto usual SEM holders and put into a box which was then sealed under argon in an aluminum bag. To maintain a low exposure to the surrounding atmosphere, the samples were opened and quickly put into the SEM directly after the chamber was opened with the entire process taking less than one minute.

Further optical post mortem analysis was carried out using a 4K light microscope (VHX-7000, Keyence, Japan).

Solid PEO-based electrolytes prepared *via* solvent-based tape casting were analyzed by dynamic differential scanning calorimetry (DSC) to investigate the melting point. Therefore, each

sample was sealed inside an aluminum crucible in the dry room and tested over a heating and cooling procedure in a DSC apparatus (DSC 3, Mettler Toledo GmbH, Switzerland). The program started with cooling to −60 °C for 255 s (at a rate of −0.333 K s^{-1}), which was kept for 120 s. Afterwards the first heating run up to 95 °C with a heating rate of 0.167 K s^{-1} was carried out. The maximum temperature was kept for 30 s. This was followed by another cooling and heating cycle. For the melting point determination always the extrapolated onset of the first heating run was evaluated.[26] The degree of crystallinity for blends composed of PEO with different molecular weights and LiTFSI or LiFSI conducting salt in different EO : Li ratios was calculated with the following equation according to our previous research,[27] where ΔH_m is the melting enthalpy of the sample, ΔH_{PEO} is the melting enthalpy of fully crystalline PEO (196.4 J g^{-1}),[28] and f_{PEO} is the mass percentage of PEO in the blend.

$$\chi = \frac{\Delta H_m}{\Delta H_{PEO} \cdot f_{PEO}} \times 100$$

2.3. Electrochemical measurements

For impedance measurements, the electrolytes made under solvent-based conditions were inserted into coin cells (GELON, 2032 type, China) in the dry room. Therefore, the electrolyte was punched into 17 mm disks and one disk each was placed directly into the bottom cover. Afterwards a 10 μm thick copper disk with a diameter of 16 mm was added. *Via* this method the thickness of the sticky electrolyte could be measured right before cell crimping. To finish cell building stainless steel spacers (1 × 0.5 mm and 2 × 0.8 mm) were added followed by a wave spring and top cover. The cell building setup can be seen in the SI, Fig. S1. Electrochemical impedance spectroscopy (EIS; Biologic, VSP300, France) was performed in a frequency range of 7 MHz to 100 mHz subsequently at 20, 50 and 80 °C for these coin cells. Always three cells for each system were built and the temperature was kept constant for 2 h before measuring EIS.

For the main investigations EL-cells instead of coin cells were fabricated. The cell assembly was performed in dry room atmosphere. The coated electrode materials and PEO electrolytes were punched out of the material sheets using a circular punching tool. The diameters of the punched cell components were as follows: cathode: 17 mm (more information regarding the S cathode as well as SEM images showing the surface structure are available in the SI, Fig. S3), anode: 18 mm, electrolyte: 19 mm. Then the cell components were placed inside a hermetically sealed modular test cell (PAT-cell, EL-Cell GmbH, Germany). For each of the investigated electrolyte thicknesses (150 μm, 300 μm and 600 μm) one test cell was assembled.

The electrical investigations of the cells were carried out with docking stations (PAT-channel-1, EL-Cell GmbH, Germany) in a temperature chamber (Binder KB 115, WKM Wärmeprozess- und Klimaprüftechnik Michel GmbH & Co. KG, Germany). The docking stations were connected to a control unit (PAT-Tester-x-8, EL-Cell GmbH, Germany). Before starting the electrical tests, the test cells were heated up to 50 °C and stored for approx. 18 hours. The temperature was maintained at 50 °C throughout the test. In a first step the test cells were discharged with 0.02 C to 1.5 V. The C-rate was referred to the calculated theoretical capacity. After the first discharge step the test cells were cycled with up to 50 loops (CCCV-charging and CC-discharging each with 0.1C) between 1.5 V and 3.0 V. The recording of the data was performed at every change of 5 mV or 5 mA.

3. Results and discussion

3.1. Preliminary parameter evaluation using solvent based electrolyte fabrication

The solid electrolyte composition showing best performance was investigated prior to upscaling to the solvent-free process under variation of PEO molecular weight, conducting salt and EO : Li ratio. In order to identify the optimal composition, electrolyte films were prepared by a solvent based tape-casting method in a dry room and subsequently analyzed by electrochemical impedance spectroscopy (EIS) and differential scanning calorimetry (DSC). For parameter evaluation five different PEO molecular weights (2000, 20 000, 200 000, 600 000 and 2000 000 Da), three conducting salts (LiTFSI, LiFSI and LiBArF) and three EO : Li ratios (10 : 1, 15 : 1 and 20 : 1) were investigated. Being one of the most studied conducting salts in the Li–S battery and SSB research fields, LiTFSI was chosen as an indispensable reference system.[29–32] As an alternative not falling under the PFAS (per- and polyfluoroalkyl substances) definition and regulations, LiFSI gained a lot of interest in recent years and promises stable SEI build-up, which leads to improved battery performance[33–35] as we could also prove in our previous research on novel liquid electrolytes for Li–S batteries.[36] LiBArF has not been used in Li–S battery research so far and seems to be a promising candidate due to its weakly coordinating anion[37] allowing high and more unhindered Li^+ movement due to the lower ionic interactions between Li cation and BArF anion.

The mechanical strength[38] and viscosity of PEO decrease with decreasing molecular weight. Thereby, it was not possible to prepare a free-standing film for the PEO materials with molecular weights of 2000 and 20 000 Da. Preparing the casting solution with a dissolver results in strong bubble formation during the process of mixing. These air bubbles (see Fig. 1a) are trapped in the highly viscous polymer solution and must be removed by vacuum (see Fig. 1b) to ensure the subsequent preparation of a complete and homogenous film.

Such desired homogeneous films were obtained for the LiTFSI and LiFSI samples (see Fig. 1c and d). In contrast, only inhomogeneous films for all EO:Li ratios of LiBArF could be fabricated (see Fig. 1e). Furthermore, it was difficult to dissolve LiBArF, and even after complete dissolution in ethanol the resulting LiBArF films after drying again showed to be inhomogeneous.

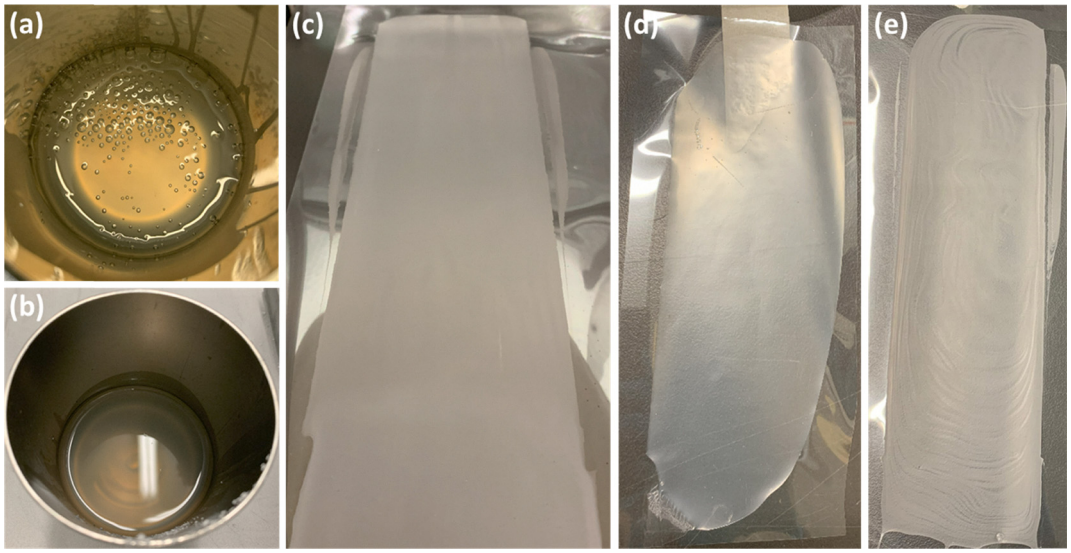

Fig. 1 Representative examples for solvent-based solid electrolyte film production. (a) Electrolyte solution with air bubbles and (b) after vacuum treatment. Solid electrolyte film on transparent substrate foil with (c) lithium bis(trifluoromethylsulfonyl)amide (LiTFSI), (d) lithium bis(fluorosulfonyl)imide (LiFSI) and (e) lithium tetrakis(pentafluorophenyl)borate (LiBArF).

The EIS data depicted in Fig. 2a, c and e shows the ionic conductivity of all systems measured at three temperatures (20, 50 and 80 °C). Being strongly temperature-dependent, the ionic conductivity increases with temperature as expected.[39,40] When comparing different PEO molecular weights, the ionic conductivity increases with decreasing molecular weight for LiTFSI based electrolytes. This finding has also been observed in other studies;[41,42] especially at lower molecular weights (<100 000 Da, especially <10 000 Da) a substantial increase of ionic conductivity was reported.[43] On the other hand, for LiFSI and LiBArF no clear trend was observed and all PEO molecular weights seem similar on average. The electrolytes with LiTFSI conducting salt show the overall highest ionic conductivity for each EO:Li ratio at all temperatures and PEO molecular weights (LiTFSI ≫ LiFSI ≫ LiBArF). LiFSI follows with a conductivity one to two orders of magnitude lower at 20 and 50 °C, but the gap closes more at 80 °C, where its conductivity is only 5–10 times lower than for LiTFSI. The conductivity of the LiBArF electrolytes is the lowest ranging from 10^{-9} S cm^{-1} to $<10^{-6}$ S cm^{-1}. Regarding the EO : Li ratio, the electrolyte system with LiTFSI follows the trend that the conductivity increases with increasing conducting salt concentration (20 : 1 < 15 : 1 < 10 : 1, EO : Li). In contrast, the conductivity of the electrolyte system with LiFSI on average increases with decreasing conducting salt content (10 : 1 < 15 : 1 < 20 : 1, EO : Li). This finding was especially observed at higher temperatures of 50 and 80 °C. LiFSI films with high conducting salt content (10 : 1, EO : Li) showed a tendency to become wrinkled or rolled up. This was not found for FSI films with the lower amounts of conducting salt. It is believed that these findings appear due to LiFSI not being fully dissociated in the polymer matrix, leading to film inhomogeneities. A similar trend of increasing conductivity with decreasing content of conducting salt was observed for the LiBArF films (10 : 1 < 15 : 1 < 20 : 1, EO : Li). In that case of this trend is probably due to the strong inhomogeneity of the LiBArF films, because of incomplete dissolution of the conducting salt and thus limited interaction of Li^+-ions in the polymer matrix. LiBArF films are not considered further below due to their very low conductivity and inhomogeneity.

The melting point of a polymer solid electrolyte has a decisive influence on the ionic conductivity. It is known that the ions are mainly transported through the amorphous regions.[44] The ionic conductivity of a semi-crystalline polymer such as PEO is therefore increased if the melting point is lowered by additives, resulting in a lower crystalline content for a given temperature.[45] DSC was used to determine the melting points (see Fig. 2b, d and f). The addition of the conducting salt leads to a significant reduction in the melting point compared to the pure PEO for all tested molecular weights. Furthermore, it can be seen that the LiFSI samples always have higher melting points and therefore a lower ionic conductivity than LiTFSI electrolytes, as a lower proportion of amorphous regions is presumably present in the LiFSI samples compared to LiTFSI in the polymer matrix. We speculate that this is due to lower interaction of the FSI anion with the polymer compared to TFSI. The increase in conducting salt content (lower EO:Li ratio) also leads to a melting point reduction in principle, which explains the observation of highest conductivities with 10 : 1 EO : Li for the LiTFSI samples. PEO 200 000 Da 10 : 1 LiTFSI is the only electrolyte for which no melting event occurred for the second heating, due to its low degree of crystallinity. To gain further insight the degree of crystallinity was calculated. Fig. 3a and b shows the degree of crystallinity for LiTFSI and LiFSI blends with PEO. The lowest degree of crystallinity was observed for PEO 200 000 Da 10 : 1 LiTFSI for the first (χ = 8.33) and second heating run (χ = 0) (see Table S1). Comparing the different molecular weights for the 10 : 1 electrolytes, similar values were only observed for the

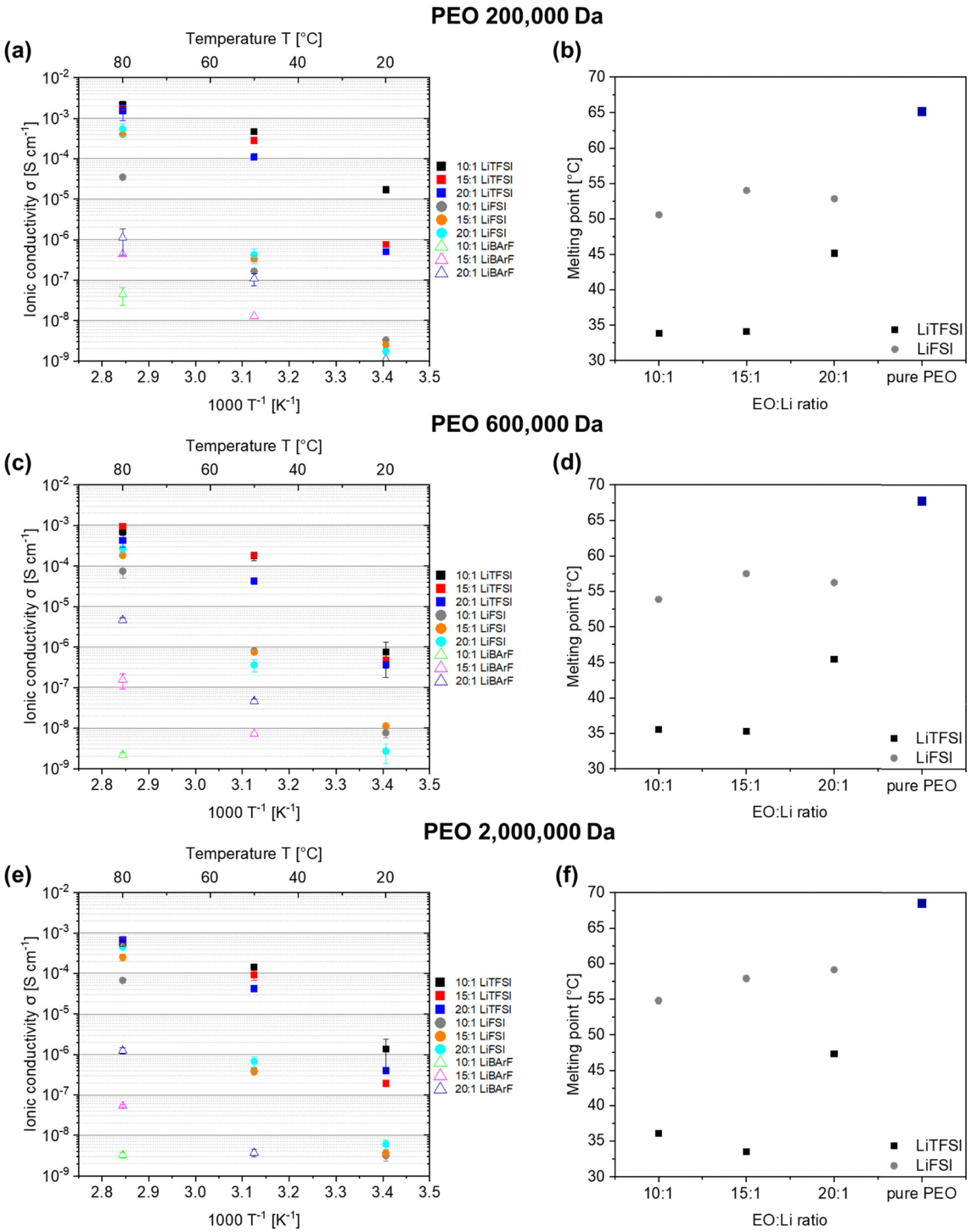

Fig. 2 Evaluation of the ionic conductivity as determined by EIS (a), (c) and (e) and the melting point obtained *via* DSC (b), (d) and (f) of the solid electrolyte films with different conducting salts (LiTFSI, LiFSI, LiBArF), Li salt concentrations (EO : Li ratio) and PEO molecular weights of 200 000, 600 000 and 2000 000 Da.

second heating run. Inconsistencies can be observed for the first heating runs of LiTFSI samples, which can be attributed to storage effects. Therefore, to circumvent the influence of storage effects only the second heating runs will be considered. Within the investigated molecular range, pure PEO samples follow the trend that crystallinity decreases with increasing molecular weight. This observation is in good agreement with the literature,[46,47] as with increasing molecular chain length entanglement and thus amorphicity increases. However, regarding PEO-LiTFSI or LiFSI blends very similar values for crystallinity were found for increasing molecular weight, whilst strong differences appear for the distinct ratios of EO : Li. As the

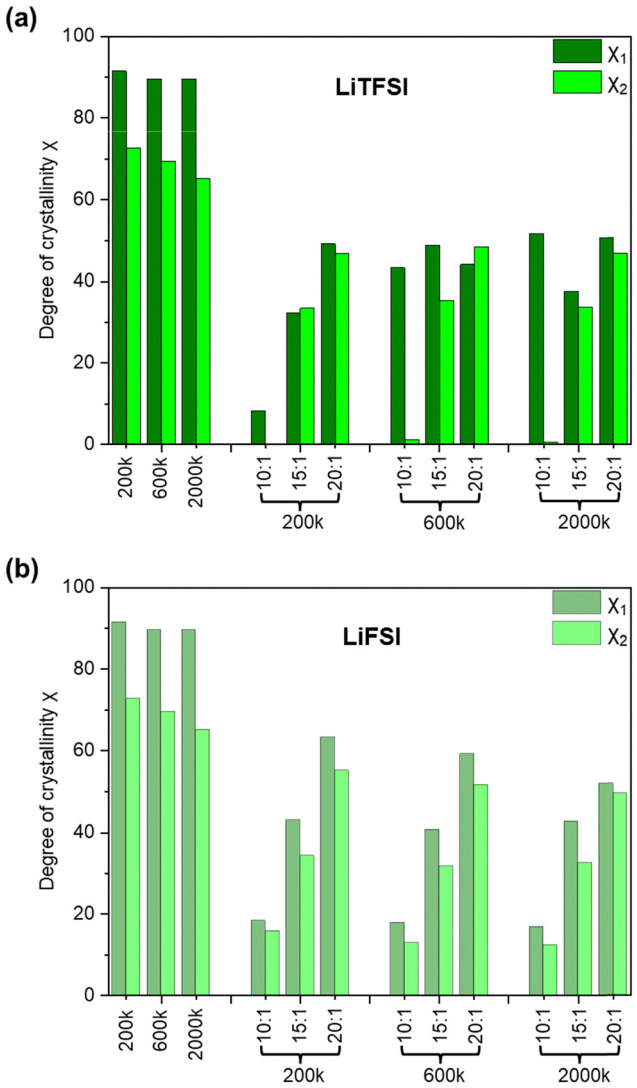

Fig. 3 Degree of crystallinity characterized by DSC for the first (χ_1) and second heating (χ_2) of pure PEO samples with the molecular weights 200 000 Da, 600 000 Da and 2000 000 and corresponding PEO-LiTFSI (a) and PEO-LiFSI blends (b) with EO : Li ratios of 10 : 1, 15 : 1 and 20 : 1, respectively.

polymer interacts with the conducting salt the crystallinity decreases with increasing salt content leading to higher ionic conductivity. However, the different trend observed above for LiFSI (see Fig. 2) is not reflected in the degree of crystallinity, showing that secondary effects like homogeneity also play a big role.

The electrolyte system PEO 200 000 Da 10 : 1 LiTFSI shows the best ionic conductivity of all tested systems (approx. 4–5 × 10^{-4} S cm^{-1} at 50 °C), but is characterized by very low mechanical stability and is extremely sticky, aggravating further processing. It was also noticed that samples with PEO 200 000 Da 10 : 1 LiTFSI crystallized after a short time (one to two days). Therefore, the decision was made to use PEO 600 000 Da with 10 : 1 LiTFSI as the best electrolyte system despite its slightly lower ionic conductivity (approx. 1–2 × 10^{-4} S cm^{-1} at 50 °C), as these films did not fully crystallize within one day and thus were more flexible, were less sticky and showed better mechanical stability. A more detailed analysis of the mechanical properties *via* nanoindentation was performed and can be found in the SI section (see S4 Investigation of mechanical properties by nanoindentation).

3.2. Solvent-free electrolyte fabrication

A simple electrolyte consisting of only PEO and LiTFSI is sufficient to enable cycling at higher temperatures like 80 °C. From the ionic conductivity data for LiTFSI in Fig. 2, it can also be suggested that galvanostatic cycling at 50 °C should be possible as the ionic conductivity is higher than 10^{-4} S cm^{-1}. However, the ionic conductivity of 10 : 1 and 15 : 1 LiTFSI for 80 °C and also 50 °C in Fig. 2 are very similar and it is unclear if 10 : 1 is already the optimum value. Comparing all PEO molecular weights, the melting point measurements suggest that the optimal value in general could lie in between. A similar outcome was observed for the LiFSI samples, where the optimal EO : Li ratio might lie in between 15 : 1 and 20 : 1 for PEO-LiFSI based films. Based on further literature research, it was decided to perform all further investigations with the LiTFSI system using a 12 : 1 EO : Li ratio instead of 10 : 1, as this represents the optimum content of LiTFSI in PEO for this temperature range.[48,49] Furthermore, under the aspect of increasing the scalability by using a kneader, a lower content of the expensive conducting salt is economically more advisable.

The kneader-based SPE fabrication was performed under dry room conditions with a total kneading time of 15 min for one batch resulting in 50 g of solvent-free solid electrolyte. Further densification by calendering is required in order to form a homogenous solid electrolyte film with a certain thickness for electrochemical investigation in EL-Cell setups (see Fig. 4a–e). Previous galvanostatic cycling tests in coin cells at 80 °C showed that a minimum thickness of the electrolyte was required for a cell to function and not short-circuit. Therefore, three different thicknesses (150, 300 and 600 μm) were evaluated for the EL-Cell experiment setup. Interestingly the solid electrolyte film remained unchanged for 3 days but crystallized after 1–2 weeks (compare Fig. 4d and f). The ionic conductivity was measured after storage and showed to be comparable to the solvent-based solid electrolytes, reaching ~2.39 × 10^{-4} S cm^{-1} at 50 °C on average for all thicknesses (see Fig. S2). Notably for 20 °C a significantly higher average ionic conductivity of ~8.12 × 10^{-6} S cm^{-1} for all thicknesses was reached.

The electrochemical cycling performance of Li–S EL-cells with the solid electrolyte PEO 600 000 Da 12 : 1 LiTFSI is presented in Fig. 5. The cell containing the electrolyte with the lowest thickness of 150 μm showed the highest initial capacity of 750 mAh g s^{-1}. However, this cell also showed strong capacity fading and malfunctioned after 14 cycles with a CE between 90–99%. With lower initial capacity and lower capacity fading but strongly increased cycle life, the cell with 300 μm thick electrolyte showed a CE of 90–99% for 17 cycles which however steadily decreased afterwards. The 600 μm thick electrolyte possessed the lowest initial capacity of

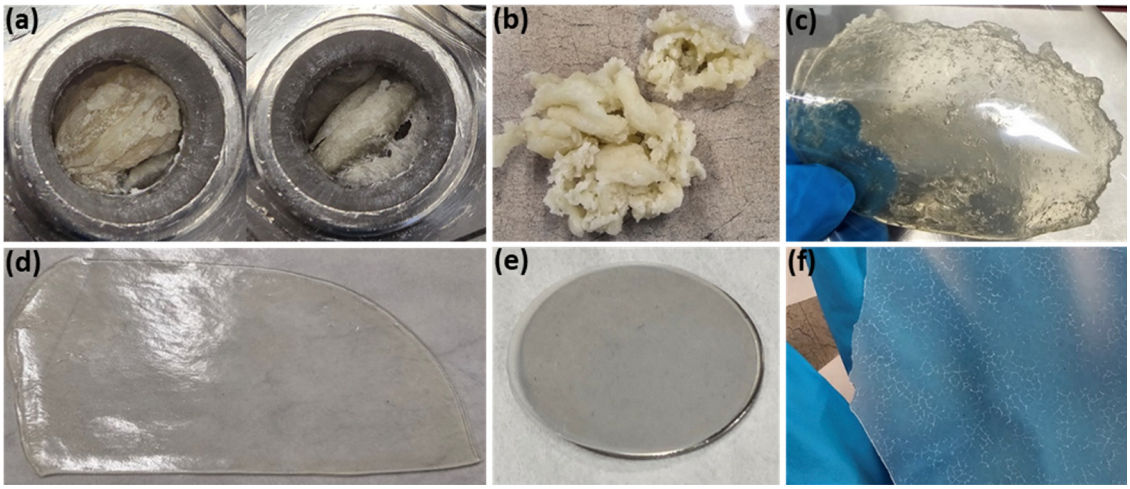

Fig. 4 Solid electrolyte consisting of PEO and LiTFSI (12 : 1, EO : Li) produced in a solvent-free manner by kneading. Photographs of (a) the kneading process, (b) 50 g solid electrolyte after kneading, (c) solid electrolyte after pre-densification by the hot press, (d) densification by the calender, (e) punched solid electrolyte on stainless steel spacer (diameter = 16 mm), (f) solid electrolyte after two weeks storage at room temperature.

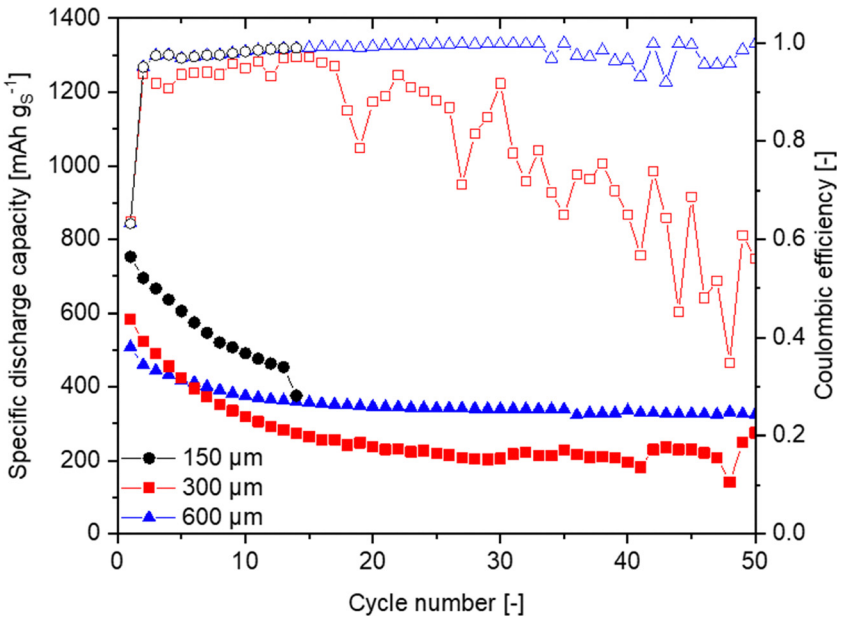

Fig. 5 Galvanostatic cycling at 50 °C of Li–S EL-cells with different solid electrolyte thicknesses (150, 300 and 600 µm). Coulombic efficiency is displayed by hollow data points.

500 mAh g s^{-1} but also the lowest capacity fading and its discharge capacity remained above 300 mAh g s^{-1} throughout the cycling procedure for 50 cycles. In terms of CE an improvement can be seen as well, with the Coulombic efficiency (CE) staying close to 100% for the whole duration of the cycling test.

A detailed description and analysis of the cathode (see Fig. S3) including a galvanostatic cycling test with the solid electrolyte at 80 °C (see Fig. S4) and a liquid electrolyte system (see Fig. S5) for comparison can be found in the SI, S2.

A comparison of the voltage-capacity profiles in Fig. 6 reveals voltage fluctuation for the charging curves of the 150 and 300 µm samples. Severe voltage fluctuation, possibly arising from micro short-circuits, can be observed for the first and last cycle of the 300 µm sample. The early malfunctioning of 150 and 300 µm samples thus is suggested to be due to dendritic growth as the cause of failure. No voltage fluctuation was observed for the thicker 600 µm electrolyte. All discharge profiles start at around 2.45 V, directly followed by the first discharge plateau which suggests the formation of longer polysulfides. This plateau has very low capacity output of less than 100 mAh g s^{-1} and becomes smaller with increasing electrolyte thickness, suggesting incomplete transformation of

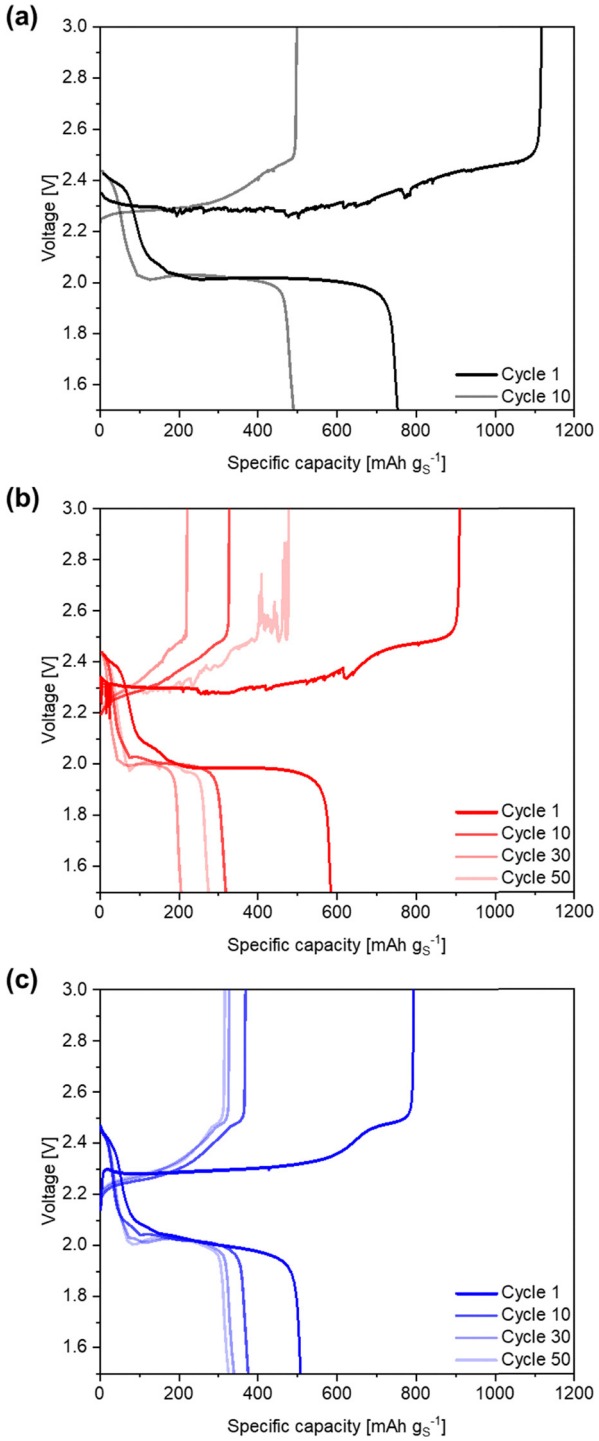

Fig. 6 Voltage–capacity profiles for the cycled Li–S EL-cells with different electrolyte thickness of (a) 150 μm, (b) 300 μm, and (c) 600 μm.

the longer polysulfides. The same trend occurs for the larger second plateau where the reduction of low-chain polysulfides to Li_2S_2 and finally Li_2S brings most of the capacity, suggesting an incomplete reaction again. A large gap between charge and discharge of the first cycle of each system can be observed, corresponding to poor initial CE. At the 10th cycle, the CE is close to 100% for 150 and 600 μm while the cell with 300 μm electrolyte thickness remained at around 95%, matching the observations discussed above. The noise visible in the 50th charge curve of the 300 μm system indicates cell malfunctioning.

A post-mortem analysis was carried out to obtain more insight and find explanations to the observed electrochemical behavior. The sticky character of the PEO-LiTFSI electrolytes complicates a separation of the cell components. For the 150 μm electrolyte, it was not possible to separate cathode from anode even after 1 h heat treatment at 60 °C (Fig. 7a and b). However, the electrodes could be separated for the cells with electrolyte thickness of 300 and 600 μm. A yellowish coloration was observed within the electrolyte which stems from the polysulfide formation as we already reported in previous studies.[36,50] The coloration quickly fades after air exposure and thus is barely visible in the pictures (Fig. 7c and d). Fig. 7e shows a comparison of the cores of two EL-cells, for the 600 and 150 μm electrolyte, respectively, after operation at 50 °C over 50 cycles. For the 600 μm electrolyte, excess electrolyte was observed to be leaking from the cell. This excess electrolyte can be also seen behind the plastic cover around the metal plunger. It is not very visible from the picture but also for the 150 μm sample a small amount of excess electrolyte was observed around the metal plunger (see Fig. 7e, red ellipse). These findings could explain the early malfunctioning and worse cycling behavior of the thinner 150 and 300 μm electrolyte samples. With a thickness reduction during cycling the possibility of dendrites short-circuiting the electrodes becomes more probable.

With the use of a 4K light microscope a deeper optical investigation was possible. Fig. S6 shows a post-mortem analysis of the lithium anode and sulfur cathode at different magnifications. During the investigation it seemed that the deep orange-colored spots are directly on the anode and covered by electrolyte (see Fig. S6a–c). It is assumed that these spots are dead sulfide species that had stopped to participate in the electrochemical reaction after binding to the anode. Around the edge of the investigated anode a gold-brownish-colored electrolyte accumulation in ring shape was discovered (Fig. S6a). An image at further magnification shows that this gold-brownish substance differs from the deep-orange colored spots and is assumed to correlate to polysulfides of higher order that had dissolved in the electrolyte (Fig. S6d); also a number of black spots can be observed (Fig. S6a and d). This might occur due to insufficient pressure around the edges and is known as the edge effect in batteries where the formation of dead Li is very likely.[51] These black spots are predominantly present close to the edge supporting this theory.

To observe the surface morphology in further detail, an SEM-supported post-mortem analysis for the best-performing system with the 600 μm electrolyte was performed. Fig. 8a–c shows the surface morphology of the electrolyte on the Li anode at different magnifications. At higher magnifications the spherulitic character of PEO becomes visible that leads to many wrinkles on the surface (see Fig. 8b). Furthermore, agglomerates ~20 μm in size can be observed. An EDX analysis

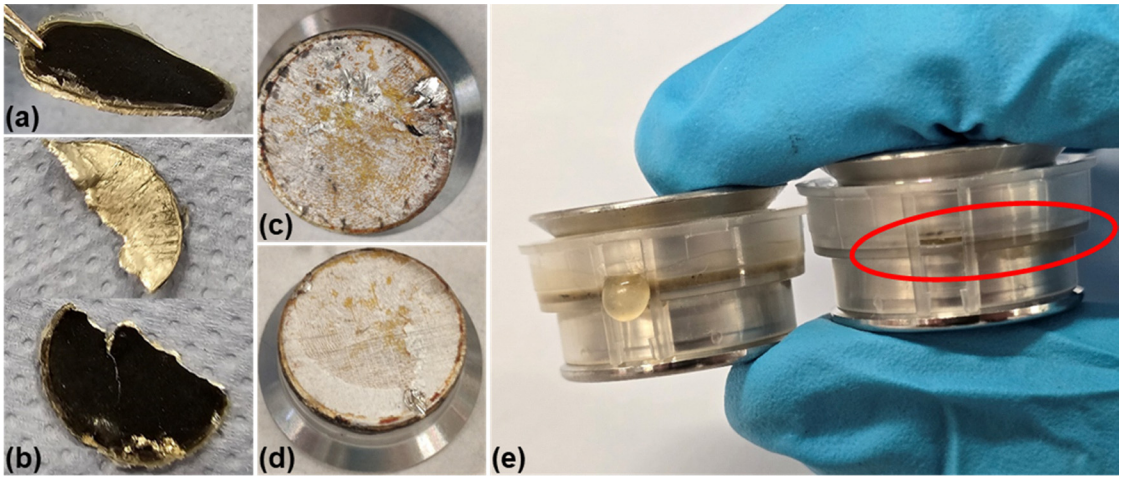

Fig. 7 Post-mortem analysis of the Li–S EL-cells after galvanostatic cycling. Photographs of (a) anode, electrolyte and cathode composite/laminate of the 150 μm sample after 14 cycles. (b) Sample breakage during delamination of the 150 μm sample. (c) Anode of the 300 μm sample after 50 cycles. (d) Anode of the 600 μm sample after 50 cycles. (e) Comparison of EL-cell core with active battery parts sandwiched between two metal plungers and a surrounding plastic gasket cover for the 600 μm sample (left) and the 150 μm sample (right).

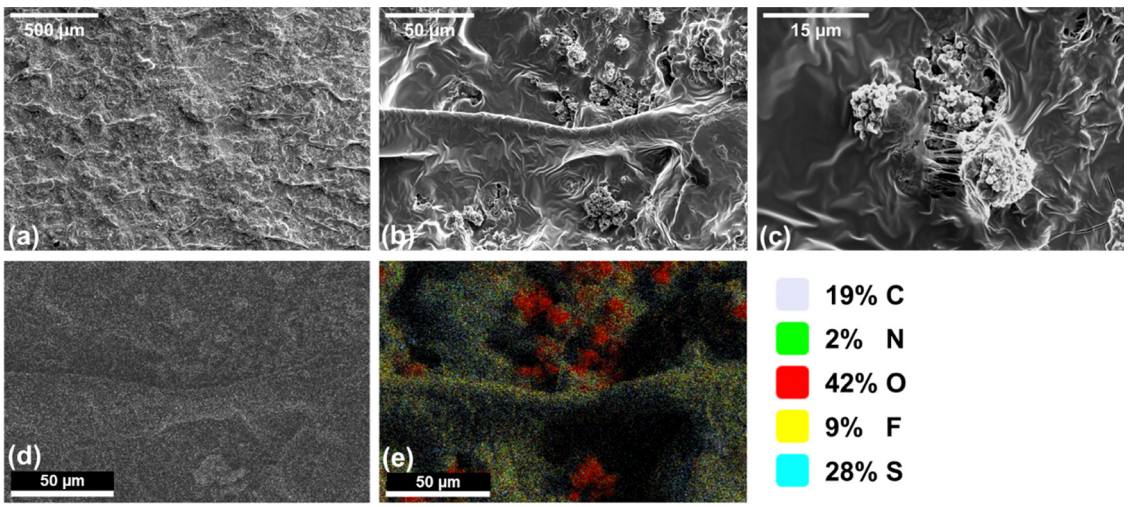

Fig. 8 SEM images of Li anode of the Li–S EL-Cell with 600 μm electrolyte thickness in post mortem analysis. Three different magnifications of (a) ×200, (b) ×2000, (c) ×8000, and (d) and (e) element mapping obtained *via* EDX analysis.

measuring C, N, O, F, S was performed as these elements can be utilized to determine the distribution of the solid electrolyte components PEO and LiTFSI as well as dissolved sulfur/polysulfides. The elemental distribution in Fig. 8e (corresponding to Fig. 8b and d) gives rise to the assumption that these agglomerates could correspond to plated Li because all of them show an enhanced content of oxygen, which is attributed to oxygen contamination that might have occurred during the sample mounting in the SEM device or during sample preparation in the dry room. A high content of S on the anode surface also explains the low capacity output due to the active material loss *via* the dissolution of polysulfides in the electrolyte and their subsequent deposition on the anode.

The SEM analysis of the sulfur cathode was executed under the same conditions as for the Li anode. Here, the different magnifications in Fig. 9 only show the electrolyte on top of the cathode that is partially ripped off, thus showing a similar rippled structure as for the Li anode. However, the rips are of much larger size and the smaller wrinkles are not observed but the image at higher magnification reveals a smooth surface in between the rips. Thus, the characteristic PEO spherulites are not observed. The 4K light microscope investigation of the cathode did not show any visible color change, in contrast to the Li anode (see Fig. S6e–h). Since the EDX analysis provides very similar values for all probed elements, with only the oxygen content being 11% lower, a similar concentration of polysulfides is expected. The only conceivable difference is the higher amount of Li in and around the electrolyte at the Li anode site that however cannot be detected *via* EDX. One possible reason could be that Li-rich PEO-LiTFSI clusters and/or the observed

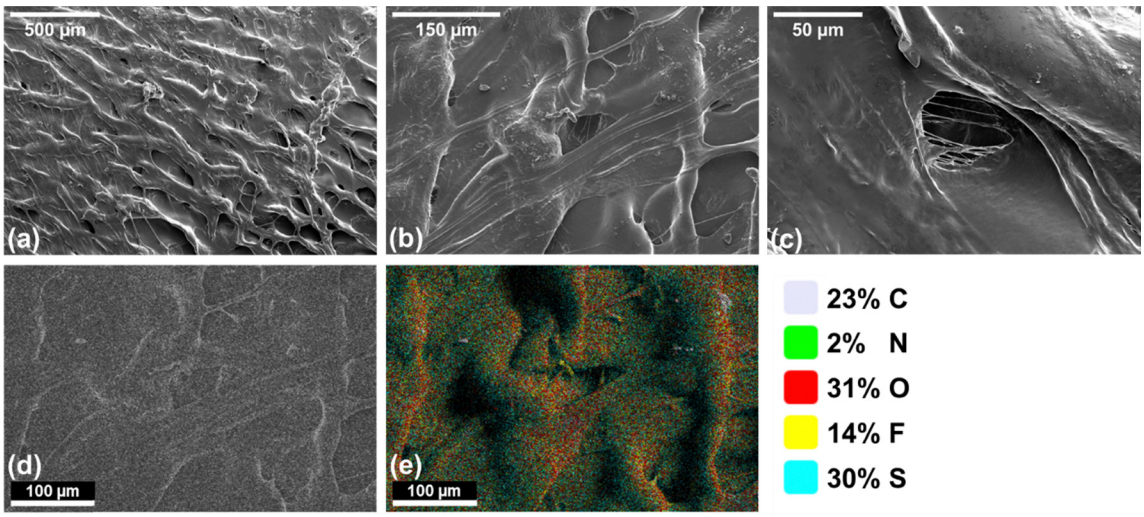

Fig. 9 SEM images of the sulfur cathode of the Li–S EL-cell with 600 µm electrolyte thickness in post-mortem analysis. Three different magnifications of (a) ×200, (b) ×800, (c) ×2000 and (d) and (e) element mapping obtained from EDX analysis.

agglomerates at the anode surface might act as nucleation sites within the PEO, increasing the crystallinity and thus forming the spherulitic PEO structure. In summary, the post mortem analysis showed that an early malfunctioning of the cells with thinner electrolyte of 150 and 300 µm might have happened due to a short-circuit induced by dendrites. The reported thickness reduction of the PEO electrolyte, which is caused by material flow due to high internal cell pressure and temperatures above the melting point, thereby enhances the probability of dendrites contacting the electrodes, especially for the thinner electrolytes.

4. Conclusion

This research described and compared a solvent-based and a solvent-free solid electrolyte preparation at larger scale under dry room conditions. Initially, *via* the solvent-based process, a detailed study on the influence of different PEO molecular weights, conducting salts and EO:Li ratios was performed. The system with the medium-molecular weight PEO (600 000 Da) and LiTFSI in a 10 : 1 ratio revealed the best performance with a combination of high ionic conductivity and mechanical strength. Based on these results, the solvent-free approach by using a kneader was established with the high-molecular weight PEO. This approach allows good scalability, and already 50 g of electrolyte could be fabricated in one batch within 15 min. The electrochemical performance was investigated by galvanostatic cycling of EL-cells with a Li metal anode and a sulfur-carbon composite cathode. Whilst thin electrolyte layers of 300 µm and less caused severe problems during cycling, a cell based on the thicker electrolyte of 600 µm exhibited good cycling stability (steady capacity during the complete test duration of 50 cycles), good coulombic efficiency (between 90 and 99%) and lowest capacity fading. Thinner PEO electrolytes result in higher initial capacity, possibly due to a lower amount of polysulfides being dissolved in the smaller volume of electrolyte present in the cell; however, they lead to greater capacity loss and malfunction probability. An SEM-supported post-mortem analysis indicated that dendritic Li plating might have caused early malfunctioning of the cells with the thinnest solid electrolyte separator. In addition, a thickness reduction of the electrolyte during cycling was detected, based on the observation that excess material had been pressed out of the EL-cell core, which further increased the probability of short-circuiting the electrodes especially for cells with thinner electrolyte layers of 150 and 300 µm.

Conclusively, it has been demonstrated that the solvent-free kneader-based production of solid PEO-based electrolytes is a viable method to avoid the use of hazardous solvents while also saving production time by avoiding the requirement of removal of excess solvent. Advanced visual post mortem analysis using SEM-EDX and 4K-Microscope has allowed deep insight into the material system, and thus can be recommended as highly promising method in further research of polymer-based lithium sulfur batteries. These results contribute to the further development of polymer electrolytes, however a substantial improvement in ionic conductivity is still necessary. Whilst PEO-based systems appear feasible for application at 50 °C with optimized composition and thickness, room-temperature automotive and aviation applications will require other polymer matrices such as cross-linked or gel polymer systems that can show substantially higher ionic conductivity.

Conflicts of interest

The authors declare no conflict of interest.

Data availability

The data that support the findings of this study have been included as part of the supplementary information.

Supplementary information is available. See DOI: https://doi.org/10.1039/d5ya00294j.

Acknowledgements

We would like to thank the German Federal Ministry of Research, Technology and Space (BMFTR) for funding within the project FestPoLiS – FKZ: 03XP0527D. We acknowledge Q.-A. Luong (Institute for Particle Technology, Technische Universität Braunschweig) for support with the experimental part of the solvent-based electrolyte preparation. The authors also thank Michael Bredekamp (Institute for Particle Technology, Technische Universität Braunschweig) for providing access to the 4K-LM device. We also thank Daniel Vogt (Institute for Particle Technology, Technische Universität Braunschweig) for general discussions on the electrochemical analysis. Moreover, the authors acknowledge Johannes Lang (Institute for Particle Technology, Technische Universität Braunschweig) for general discussions on the differential scanning calorimetry analysis. Regarding nanoindentation measurements the authors thank Stephanie Michel and Ingo Kampen (Institute for Particle Technology, Technische Universität Braunschweig). Moreover, we acknowledge the Open Access Publication funds of Technische Universität Braunschweig for financial support of the publication.

References

1 D. Wang, L.-J. Jhang, R. Kou, M. Liao, S. Zheng, H. Jiang, P. Shi, G.-X. Li, K. Meng and D. Wang, *Nat. Commun.*, 2023, **14**, 1895.
2 M. M. Thackeray, C. Wolverton and E. D. Isaacs, *Energy Environ. Sci.*, 2012, **5**, 7854–7863.
3 B. Liu, R. Fang, D. Xie, W. Zhang, H. Huang, Y. Xia, X. Wang, X. Xia and J. Tu, *Energy Environ. Mater.*, 2018, **1**, 196–208.
4 D. A. Dornbusch, R. P. Viggiano, J. W. Connell, Y. Lin and V. F. Lvovich, *Electrochim. Acta*, 2022, **403**, 139406.
5 S. Dörfler, S. Walus, J. Locke, A. Fotouhi, D. J. Auger, N. Shateri, T. Abendroth, P. Härtel, H. Althues and S. Kaskel, *Energy Technol.*, 2021, **9**, 2000694.
6 J. Robinson and S. Gifford, *Lithium-sulfur batteries: lightweight technology for multiple sectors*, 2020, https://discovery.ucl.ac.uk/id/eprint/10112086/.
7 J. W. Fergus, *J. Power Sources*, 2010, **195**, 4554–4569.
8 S. Chen, K. Wen, J. Fan, Y. Bando and D. Golberg, *J. Mater. Chem. A*, 2018, **6**, 11631–11663.
9 X. Liang, L. Wang, X. Wu, X. Feng, Q. Wu, Y. Sun, H. Xiang and J. Wang, *J. Energy Chem.*, 2022, **73**, 370–386.
10 Q. Zhu, C. Ye and D. Mao, *Nanomaterials*, 2022, **12**, 3612.
11 C. Xian, Q. Wang, Y. Xia, F. Cao, S. Shen, Y. Zhang, M. Chen, Y. Zhong, J. Zhang, X. He, X. Xia, W. Zhang and J. Tu, *Small*, 2023, **19**, e2208164.
12 N. Verdier, G. Foran, D. Lepage, A. Prébé, D. Aymé-Perrot and M. Dollé, *Polymers*, 2021, **13**, 323.
13 Y. Nikodimos, M. Ihrig, B. W. Taklu, W.-N. Su and B. J. Hwang, *Energy Storage Mater.*, 2023, **63**, 103030.
14 L. Froboese, L. Groffmann, F. Monsees, L. Helmers, T. Loellhoeffel and A. Kwade, *J. Electrochem. Soc.*, 2020, **167**, 20558.
15 L. Xu, Y. Lu, C.-Z. Zhao, H. Yuan, G.-L. Zhu, L.-P. Hou, Q. Zhang and J.-Q. Huang, *Adv. Energy Mater.*, 2021, **11**, 2002360.
16 M. Keppeler, H.-Y. Tran and W. Braunwarth, *Energy Technol.*, 2021, **9**, 2100132.
17 C. Wang, Y. Yang, X. Liu, H. Zhong, H. Xu, Z. Xu, H. Shao and F. Ding, *ACS Appl. Mater. Interfaces*, 2017, **9**, 13694–13702.
18 B. Guo, Y. Fu, J. Wang, Y. Gong, Y. Zhao, K. Yang, S. Zhou, L. Liu, S. Yang, X. Liu and F. Pan, *Chem. Commun.*, 2022, **58**, 8182–8193.
19 G. Piana, F. Bella, F. Geobaldo, G. Meligrana and C. Gerbaldi, *J. Energy Storage*, 2019, **26**, 100947.
20 C. Li, H. Yue, Q. Wang and S. Yang, *Russ. J. Electrochem.*, 2022, **58**, 271–283.
21 X. Zhang, C. Fu, S. Cheng, C. Zhang, L. Zhang, M. Jiang, J. Wang, Y. Ma, P. Zuo, C. Du, Y. Gao, G. Yin and H. Huo, *Energy Storage Mater.*, 2023, **56**, 121–131.
22 K. Khan, M. B. Hanif, H. Xin, A. Hussain, H. G. Ali, B. Fu, Z. Fang, M. Motola, Z. Xu and M. Wu, *Small*, 2024, **20**, e2305772.
23 L. Zhao, M. Hou, K. Ren, D. Yang, F. Li, X. Yang, Y. Zhou, D. Zhang, S. Liu, Y. Lei and F. Liang, *Small Methods*, 2024, **8**, e2301579.
24 L. Froboese, J. F. van der Sichel, T. Loellhoeffel, L. Helmers and A. Kwade, *J. Electrochem. Soc.*, 2019, **166**, A318–A328.
25 L. Helmers, L. Froböse, K. Friedrich, M. Steffens, D. Kern, P. Michalowski and A. Kwade, *Energy Technol.*, 2021, **9**, 2000923.
26 R. Riesen, *Einfluss der Heizrate: Schmelzen und chemische Reaktion*, 2006.
27 E. J. Jeon, S. Haidar, L. Helmers, A. Kwade and G. Garnweitner, *Energy Adv.*, 2024, **3**, 2428–2438.
28 N. A. Stolwijk, C. Heddier, M. Reschke, M. Wiencierz, J. Bokeloh and G. Wilde, *Macromolecules*, 2013, **46**, 8580–8588.
29 H. Zhang, C. Liu, L. Zheng, F. Xu, W. Feng, H. Li, X. Huang, M. Armand, J. Nie and Z. Zhou, *Electrochim. Acta*, 2014, **133**, 529–538.
30 M. Huang, S. Feng, W. Zhang, L. Giordano, M. Chen, C. V. Amanchukwu, R. Anandakathir, Y. Shao-Horn and J. A. Johnson, *Energy Environ. Sci.*, 2018, **11**, 1326–1334.
31 A. Santiago, J. Castillo, I. Garbayo, A. Saenz de Buruaga, J. A. Coca Clemente, L. Qiao, R. Cid Barreno, M. Martinez-Ibañez, M. Armand, H. Zhang and C. Li, *ACS Appl. Energy Mater.*, 2021, **4**, 4459–4464.
32 Z. Li, L. Wang, X. Huang and X. He, *Adv. Funct. Mater.*, 2024, **34**, 2408319.
33 H.-B. Han, S.-S. Zhou, D.-J. Zhang, S.-W. Feng, L.-F. Li, K. Liu, W.-F. Feng, J. Nie, H. Li and X.-J. Huang, *J. Power Sources*, 2011, **196**, 3623–3632.
34 G. G. Eshetu, X. Judez, C. Li, M. Martinez-Ibañez, I. Gracia, O. Bondarchuk, J. Carrasco, L. M. Rodriguez-Martinez,

H. Zhang and M. Armand, *J. Am. Chem. Soc.*, 2018, **140**, 9921–9933.
35 Y. Cai, H. Zhang, Y. Cao, Q. Wang, B. Cao, Z. Zhou, F. Lv, W. Song, D. Duo and L. Yu, *J. Power Sources*, 2022, **535**, 231481.
36 N. L. Grotkopp, M. Horst and G. Garnweitner, *Battery Energy*, 2024, **3**, 20240002.
37 S. Hollstein, P. Erdmann, A. Ulmer, H. Löw, L. Greb and M. von Delius, *Angew. Chem., Int. Ed.*, 2023, **62**, e202304083.
38 A.-Y. Jee, H. Lee, Y. Lee and M. Lee, *Chem. Phys.*, 2013, **422**, 246–250.
39 Q. Ma, X. Qi, B. Tong, Y. Zheng, W. Feng, J. Nie, Y.-S. Hu, H. Li, X. Huang, L. Chen and Z. Zhou, *ACS Appl. Mater. Interfaces*, 2016, **8**, 29705–29712.
40 A. Maurel, M. Armand, S. Grugeon, B. Fleutot, C. Davoisne, H. Tortajada, M. Courty, S. Panier and L. Dupont, *J. Electrochem. Soc.*, 2020, **167**, 70536.
41 C. Papamichail, O. Techlemtzi, G. Nikolakakou and E. Glynos, *ACS Macro Lett.*, 2025, **14**, 225–230.
42 D. Devaux, R. Bouchet, D. Glé and R. Denoyel, *Solid State Ionics*, 2012, **227**, 119–127.
43 A. A. Teran, M. H. Tang, S. A. Mullin and N. P. Balsara, *Solid State Ionics*, 2011, **203**, 18–21.
44 M. Marzantowicz, J. R. Dygas, F. Krok, Z. Florjańczyk and E. Zygadło-Monikowska, *Electrochim. Acta*, 2007, **53**, 1518–1526.
45 P. Vadhva, J. Hu, M. J. Johnson, R. Stocker, M. Braglia, D. J. L. Brett and A. J. E. Rettie, *ChemElectroChem*, 2021, **8**, 1930–1947.
46 Y. Yang, M. Chen, H. Li and H. Li, *Eur. Polym. J.*, 2018, **107**, 303–307.
47 X. Chen, G. Hou, Y. Chen, K. Yang, Y. Dong and H. Zhou, *Polym. Test.*, 2007, **26**, 144–153.
48 R. Bakar, S. Darvishi, U. Aydemir, U. Yahsi, C. Tav, Y. Z. Menceloglu and E. Senses, *ACS Appl. Energy Mater.*, 2023, **6**, 4053–4064.
49 M. Wirtz, M. Linhorst, P. Veelken, H. Tempel, H. Kungl, B. M. Moerschbacher and R.-A. Eichel, *Electrochem. Sci. Adv.*, 2021, **1**, e2000029.
50 N. L. Grotkopp, M. Horst, M. Batzer, G. Garnweitner and A. Jean-Fulcrand, *Adv. Energy Sustainability Res.*, 2023, **4**, 2200146.
51 H. Lee, S. Chen, X. Ren, A. Martinez, V. Shutthanandan, M. Vijayakumar, K. S. Han, Q. Li, J. Liu, W. Xu and J.-G. Zhang, *ChemSusChem*, 2018, **11**, 3821–3828.